

# AirVO: An Illumination-Robust Point-Line Visual Odometry

Kuan Xu<sup>1</sup>, Yuefan Hao<sup>2</sup>, Chen Wang<sup>3</sup>, Lihua Xie<sup>1</sup>, *Fellow, IEEE*

**Abstract**—Visual odometry is crucial for many robotic tasks such as autonomous exploration and path planning. Despite many progresses, existing methods are still not robust enough to dynamic illumination environments. In this paper, we present AirVO, an illumination-robust and accurate stereo visual odometry system based on point and line features. To be robust to illumination variation, we introduce the learning-based feature extraction and matching method and design a novel VO pipeline, including feature tracking, triangulation, key-frame selection, and graph optimization etc. We also employ long line features in the environment to improve the accuracy of the system. Different from the traditional line processing pipelines in visual odometry systems, we propose an illumination-robust line tracking method, where point feature tracking and distribution of point and line features are utilized to match lines. In the experiments, the proposed system is extensively evaluated in environments with dynamic illumination and the results show that it achieves superior performance to the state-of-the-art algorithms.

## I. INTRODUCTION

Due to the accuracy and low-cost, visual odometry (VO) has been used in an extensive range of applications, especially in the domain of augmented reality (AR) and robotics [1]. Despite that many excellent solutions such as MSCKF [2], VINS-Mono [3] and OKVIS [4], have been proposed, the existing solutions are not robust enough to long-term applications [5]. For example, in dynamic illumination environments, visual tracking becomes more challenging and thus the quality of the estimated trajectory is severely affected [6].

On the other hand, convolutional neural network (CNN) has made great progress in many computer vision tasks, which has triggered another research trend [7]. A lot of learning-based feature extraction and matching methods have been proposed and achieve excellent performance in many applications [8]–[11]. However, they often require huge computing resource and are impractical for real-time applications with low power robots such as unmanned aerial vehicles. Therefore, we resort to a hybrid solutions that combines the efficiency of traditional optimization and the robustness of learning-based methods.

In this paper, we propose AirVO, an illumination-robust and accurate stereo visual odometry, based on learning-based feature extraction and matching algorithms. Comparing with

\*This research is supported by the National Research Foundation, Singapore under its Medium Sized Center for Advanced Robotics Technology Innovation.

<sup>1</sup>Kuan Xu and Lihua Xie are with School of Electrical and Electronic Engineering, Nanyang Technological University, 50 Nanyang Avenue, Singapore 639798 {kuan.xu, elhxie}@ntu.edu.sg

<sup>2</sup>Yuefan Hao is with the Robot R&D Department, Geekplus Corp., Beijing 100107, China yuefan.hao@outlook.com

<sup>3</sup>Chen Wang is with Department of Computer Science & Engineering, State University of New York at Buffalo, Buffalo, NY 14260, USA chenwang@dr.com

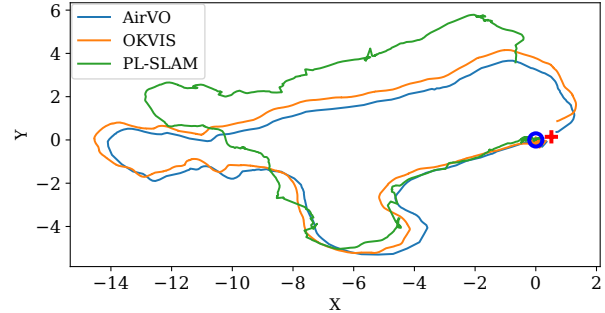


Fig. 1: Trajectories on UMA-VI conference-csc2 sequence. The blue circle and red cross are respectively the beginning and ending of the sequence acquired from ground truth.

handcrafted features used in VO or SLAM such as FAST [12] and ORB [13], learning-based features have showed better robustness to large illumination variation [9], [14], [15]. In the feature tracking stage, learning-based methods can use both appearance and geometric information of features, so it can achieve better performance than traditional data association methods such as optical flow tracking and minimizing feature descriptor distance [11]. To better apply learning-based methods to our system, we improve frame tracking, feature triangulation, and key-frame selection. To improve the accuracy, we employ line features and propose a novel line processing pipeline to make the line tracking robust to changing light conditions. Finally, a traditional SLAM backend is utilized to optimize the local map. Overall, our contributions are as follows:

- We introduce a stereo visual odometry based on learning-based feature point extraction and matching methods and line features, which is very robust and accurate in dynamic illumination environments.
- We propose a new line matching method, where we employ the point matching and the distribution of feature points and lines, to make the line tracking robust to changing light conditions.
- We accelerate the feature extraction and matching network using Nvidia TensorRT Toolkit, making our system be able to run in real time. All of our source code is available at <https://github.com/xukuanHIT/AirVO>.
- We perform experiments on challenging datasets and compare our method with the state-of-the-art methods. As shown in Fig. 1, the results demonstrate the effectiveness of our method.

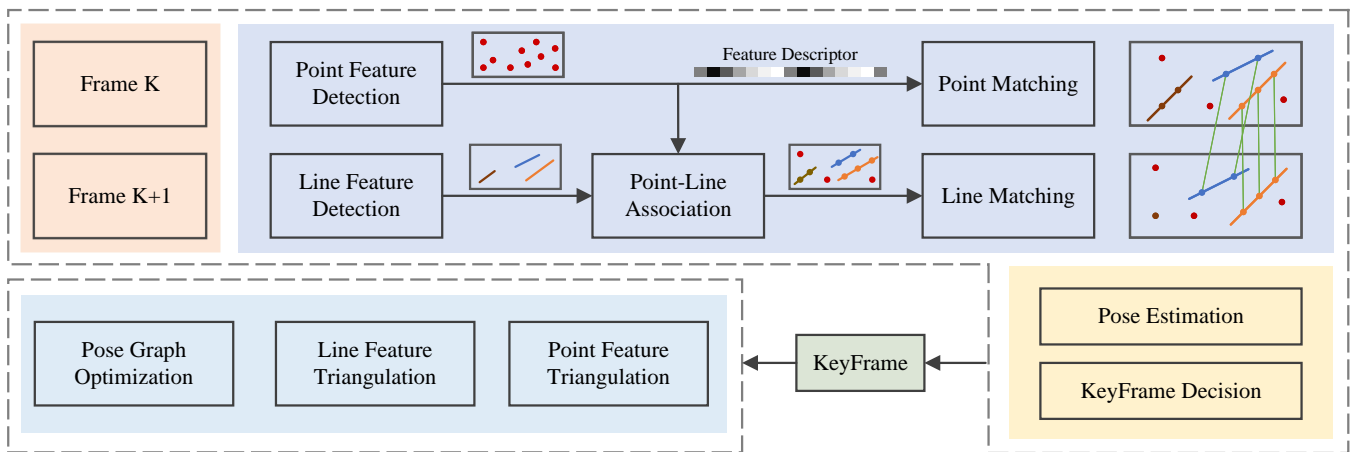


Fig. 2: The framework of AirVO. We resort to a hybrid solution that combines the efficiency of traditional optimization and the robustness of learning-based methods.

## II. RELATED WORKS

### A. Feature Extraction and Tracking for Visual SLAM

Various key-point features have been proposed and applied to different computer vision tasks. Many of these features, e.g., ORB [13], FAST [12], and BRISK [16] are applied to VO and SLAM systems, e.g., ORB-SLAM [17], VINS-Mono [3], because of their balanced effectiveness and efficiency. Two methods are widely used to track the feature points. The first is to use optical flow [3], [18], and the other is matching by descriptor [2], [19]. However, most of SLAM systems based on the above methods are evaluated in well-lighted environments and make a brightness consistency assumption. Thereby, they are significantly affected by challenging lighting conditions, such as dark, over-bright or dynamic illumination conditions.

With the development of deep learning techniques, many learning based feature extraction and matching methods have been proposed and started to be applied to visual SLAM. Kang *et al.* [20] introduce TFeat network [21] to extract descriptors for FAST corners in a traditional VSLAM pipeline. Tang *et al.* [22] use a neural network to extract robust keypoints and binary feature descriptors with the same shape of the ORB. Han *et al.* [23] combine SuperPoint [9] feature extractor with a traditional back-end. Bruno *et al.* proposed LIFT-SLAM [24], where they use LIFT [8] to extract features. Li *et al.* [15] replace ORB feature with SuperPoint in ORB-SLAM2 and optimize the feature extraction with Intel OpenVINO toolkit. However, the above methods still adopt traditional methods to track or match these learning-based features, making them not robust enough to changing illumination. Sarlin *et al.* propose HF-Net [14], where they integrate SuperPoint and SuperGlue [11] into COLMAP [25], a structure from motion (SFM) software. HF-Net achieves a good performance for visual place recognition (VPR) task but requires huge computing resources and is not able to build map in real time.

Different from current methods, AirVO introduces both learning-based feature extraction and matching methods in the VO system. By accelerating the CNN part, our system can perform pose estimation and build map in real time.

### B. Line Matching for Visual SLAM

Line features widely exist in man-made environments, which can provide additional constraints. One of the challenges of using lines in visual SLAM is to perform line matching. A method used in many current SLAM systems [26]–[30] is to match lines through LBD [31] descriptor. This method may make the line matching fail as the traditional line detection method, such as LSD [32], may be unstable. To overcome this, some systems [33]–[35] sample some points on a line, and then track the line by tracking these points. However, using either minimizing photometric error along the epipolar line or ZNCC (Zero-normalized cross-correlation) matching method [36] can't ensure robust line tracking in dynamic illumination environments.

### C. Visual SLAM for Dynamic Illumination

Several methods have been proposed to improve the robustness of VO and SLAM to illumination changes. [37]–[39] model local or global brightness changes and jointly optimize camera poses and photometric parameters. [40]–[42] try different methods, such as ZNCC and dense descriptor computation, to achieve robust planar template tracking. [43]–[45] utilize image enhancement to pre-process input images. These methods mainly focus on either global or local illumination change for all kinds of images, however, lighting conditions often affect the scene differently in different areas [46].

Other related methods include that of Huang and Liu [47], which presents a multi-feature extraction algorithm to extract two kinds of image features when a single-feature algorithm fails to extract enough feature points. Kim *et al.* [48] employ a patch-based affine illumination model during direct motion estimation. Chen *et al.* [49] minimize the Normalized Information Distance (NID) with nonlinear least square optimization for image registration.

## III. METHODOLOGY

### A. System Overview

The proposed framework is shown in Fig. 2. It's a hybrid VO system where we utilize both learning-based frontend and

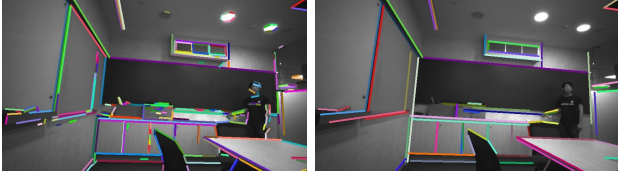


Fig. 3: Lines detected by LSD (left) and by AirVO (right).

traditional optimization backend. For every stereo image pair, we first employ a CNN (e.g., SuperPoint) to extract feature points and match them with a feature matching network (e.g., SuperGlue). We skip the details of key-point detection and matching networks, which are pre-trained models. Line features are also utilized in our system to improve the accuracy. Observing that many key-points extracted in our system lie on edges, where line features are detected, the two kinds of features are associated according to their distances. Then lines on stereo images or different frames can be matched or tracked using the matching results of their associated points for better illumination robustness. To improve the system efficiency, we only perform feature tracking on left images for different frames. Based on the feature tracking result, we select key-frames and optimize points, lines and these key-frames with bundle adjustment. The hybrid system can combine the efficiency of traditional optimization and the robustness of learning-based methods.

### B. 2D Line Processing

We first give the details of 2D line processing in our system, which includes the line segment detection and matching.

1) *Detection*: Line detection of AirVO is based on a traditional method (i.e., LSD [32]) for efficiency. LSD is a popular line detection algorithm. However, it suffers from the problem of dividing a line into multiple segments. Therefore, we improve it by merging two line segments  $\mathbf{l}_1$  and  $\mathbf{l}_2$  if the following conditions are satisfied:

- The angular difference of  $\mathbf{l}_1$  and  $\mathbf{l}_2$  is smaller than a given threshold  $\delta_\theta$ .
- The distance between the midpoint of one line and the other line is not greater than a certain value  $\delta_d$ .
- If projections of  $\mathbf{l}_1$  and  $\mathbf{l}_2$  on  $\mathbf{X}$ -coordinate axis and  $\mathbf{Y}$ -coordinate axis don't have overlap, the distance of the two closest endpoints is smaller than a certain value  $\delta_{ep}$ .

The line features detected in our system and comparison with LSD are shown in Fig. 3. We argue that long line segments are more repetitive and less affected by noise than the short ones, so after the merge, line segments whose lengths are less than a preset threshold will be filtered out so that only long line segments are used in the following stages.

2) *Matching*: Most of current VO and SLAM systems use LBD descriptor or tracking sample points to match or track lines. They perform well in good lighting conditions but suffer from the problem of changing illumination. To overcome this, we design a novel line matching pipeline for dynamic illumination environments. First, we associate point features with line segments through the distances between points and lines. Assume that  $M$  key-points and  $N$  line



Fig. 4: Line matching of AirVO in challenging scenes. Matched lines are drawn in the same color. Circles on a line are the points associated with the line. A larger radius refers that the point is associated with more lines.

segments are detected on the image, where each point is denoted as  $\mathbf{p}_i = (x_i, y_i)$  and each line segment is denoted as  $\mathbf{l}_j = (A_j, B_j, C_j, x_{j,1}, y_{j,1}, x_{j,2}, y_{j,2})$ , where  $(A_j, B_j, C_j)$  are line parameters of  $\mathbf{l}_j$  and  $(x_{j,1}, y_{j,1}, x_{j,2}, y_{j,2})$  are the endpoints. We first compute the distance between  $\mathbf{p}_i$  and  $\mathbf{l}_j$  through:

$$d_{ij} = d(\mathbf{p}_i, \mathbf{l}_j) = \frac{|A_j \cdot x_i + B_j \cdot y_i + C_j|}{\sqrt{A_j^2 + B_j^2}}. \quad (1)$$

If  $d_{ij} < 3$  and the projection of  $\mathbf{p}_i$  on the coordinate axis lies within the projections of line segment endpoints, i.e.,  $\min(x_{j,1}, x_{j,2}) \leq x_i \leq \max(x_{j,1}, x_{j,2})$  or  $\min(y_{j,1}, y_{j,2}) \leq y_i \leq \max(y_{j,1}, y_{j,2})$ , we will say  $\mathbf{p}_i$  belongs to  $\mathbf{l}_j$ . Then the line segments on two images can be matched based on the point matching result of these two images. For  ${}^k\mathbf{l}_m$  on image  $k$  and  ${}^{k+1}\mathbf{l}_n$  on image  $k+1$ , we compute a score to represent the confidence of that they are the same line:

$$S_{mn} = \frac{N_{pm}}{\min({}^kN_m, {}^{k+1}N_n)}, \quad (2)$$

where  $N_{pm}$  is matching number between point features belonging to  ${}^k\mathbf{l}_m$  and point features belonging to  ${}^{k+1}\mathbf{l}_n$ .  ${}^kN_m$  and  ${}^{k+1}N_n$  are the numbers of point features belonging to  ${}^k\mathbf{l}_m$  and  ${}^{k+1}\mathbf{l}_n$ , respectively. If  $S_{mn} > \delta_S$  and  $N_{pm} > \delta_N$ , where  $\delta_S$  and  $\delta_N$  are two preset thresholds, we will regard  ${}^k\mathbf{l}_m$  and  ${}^{k+1}\mathbf{l}_n$  as the same line.

Because the point matching is illumination-robust and feature association is not affected by lighting changes, so the proposed line tracking method is very robust to dynamic illumination environments as shown in Fig. 4.

### C. 3D Line Processing

In this part, we will introduce our 3D line processing methods. Compare with 3D points, 3D lines have more degrees of freedom, so we first introduce their representations in different stages. Then the methods of line triangulation, i.e., converting 2D line segments to 3D lines, and line re-projection, i.e., projecting 3D line to image plane, will be illustrated in detail.

1) *Representation*: We use Plücker coordinate to represent a 3D spatial line:

$$\mathbf{L} = \begin{bmatrix} \mathbf{n} \\ \mathbf{v} \end{bmatrix} \in \mathbb{R}^6, \quad (3)$$

where  $\mathbf{v}$  is the direction vector of the line and  $\mathbf{n}$  is the normal vector of the plane determined by the line and the origin [50]. Plücker coordinate is used for 3D line triangulation, transformation, and projection to the image. It's over parameterized because it's a 6-dimensional vector but a 3D line has only four degrees of freedom. In the graph optimization stage, the extra degrees of freedom will increase the computational cost and cause the numerical instability of the system [27]. Therefore, we also use orthonormal representation [50] to represent a 3D line:

$$(\mathbf{U}, \mathbf{W}) \in SO(3) \times SO(2) \quad (4)$$

The relationship of Plücker coordinate and orthonormal representation is similar to  $SO(3)$  and  $so(3)$ . Orthonormal representation can be obtained from Plücker coordinate by:

$$\mathbf{L} = [\mathbf{n} \mid \mathbf{v}] = \underbrace{\begin{bmatrix} \frac{\mathbf{n}}{\|\mathbf{n}\|} & \frac{\mathbf{v}}{\|\mathbf{v}\|} & \frac{\mathbf{n} \times \mathbf{v}}{\|\mathbf{n} \times \mathbf{v}\|} \end{bmatrix}}_{\mathbf{U} \in SO(3)} \underbrace{\begin{bmatrix} \|\mathbf{n}\| & & \\ & \|\mathbf{v}\| & \\ & & \Sigma_{3 \times 2} \end{bmatrix}}_{\Sigma_{3 \times 2}}, \quad (5)$$

where  $\Sigma_{3 \times 2}$  is a diagonal matrix and its two non-zero entries defined up to scale can be represented by an  $SO(2)$  matrix, i.e.,  $\mathbf{W}$ . In practice, this conversion can be done with the QR decomposition.

2) *Triangulation*: Triangulation is to initialize a 3D line from two or more 2D line observations. Two methods are used to triangulate a 3D line in our system. The first is similar to the line triangulation algorithm  $B$  in [28], where a 3D line can be computed from two planes. To achieve this, we select two line segments,  $\mathbf{l}_1$  and  $\mathbf{l}_2$ , on two images, which are two observations of a 3D line.  $\mathbf{l}_1$  and  $\mathbf{l}_2$  can be back-projected to two planes,  $\pi_1$  and  $\pi_2$ . Then the 3D line can be regarded as the intersection of  $\pi_1$  and  $\pi_2$ .

However, triangulating a 3D line is more difficult than triangulating a 3D point, because it suffers more from degenerate motions [28]. Therefore, we also employ a second line triangulation method if the above method fails, where points are utilized to compute the 3D line. In Section III-B.2, we have associated point features with line features. So to initialize a 3D line, two triangulated points  $\mathbf{X}_1$  and  $\mathbf{X}_2$ , which belong to this line and have the shortest distance on image plane, are selected, where  $\mathbf{X}_1 = (x_1, y_1, z_1)$  and  $\mathbf{X}_2 = (x_2, y_2, z_2)$ . Then the Plücker coordinate of this line can be obtained through:

$$\mathbf{L} = \begin{bmatrix} \mathbf{n} \\ \mathbf{v} \end{bmatrix} = \begin{bmatrix} \mathbf{X}_1 \times \mathbf{X}_2 \\ \frac{\mathbf{X}_1 - \mathbf{X}_2}{\|\mathbf{X}_1 - \mathbf{X}_2\|} \end{bmatrix}. \quad (6)$$

Because the selected 3D points have been triangulated in the point triangulating stage, so this method requires little extra computation. It is very efficient and robust.

3) *Re-projection*: We use Plücker coordinate to transform and re-project 3D lines. First, we convert the 3D line from the world frame to the camera frame:

$${}^c\mathbf{L} = \begin{bmatrix} {}^c\mathbf{n} \\ {}^c\mathbf{v} \end{bmatrix} = \begin{bmatrix} {}^c\mathbf{R} & [{}^c_w\mathbf{t}]_{\times} {}^c\mathbf{R} \\ \mathbf{0} & {}^c\mathbf{R} \end{bmatrix} \begin{bmatrix} {}^w\mathbf{n} \\ {}^w\mathbf{v} \end{bmatrix} = {}^c_w\mathbf{H} {}^w\mathbf{L}, \quad (7)$$

where  ${}^c\mathbf{L}$  and  ${}^w\mathbf{L}$  are Plücker coordinate of 3D line in the camera frame and world frame, respectively.  ${}^c_w\mathbf{R} \in SO(3)$  is the rotation matrix from world frame to camera frame and  ${}^c_w\mathbf{t} \in \mathbb{R}^3$  is the translation vector.  $[\cdot]_{\times}$  denotes the skew-symmetric matrix of a vector and  ${}^c_w\mathbf{H}$  donates the transformation matrix of 3D line from world frame to camera frame.

Then the 3D line  ${}^c\mathbf{L}$  can be projected to the image plane through a line projection matrix  ${}^i\mathbf{P}$ :

$${}^i\mathbf{l} = \begin{bmatrix} A \\ B \\ C \end{bmatrix} = {}^i\mathbf{P} {}^c\mathbf{L}_{[:3]} = \begin{bmatrix} f_x & 0 & 0 \\ 0 & f_y & 0 \\ -f_y c_x & -f_x c_y & f_x f_y \end{bmatrix} {}^c\mathbf{n}, \quad (8)$$

where  ${}^i\mathbf{l} = [A \ B \ C]^T$  is the re-projected 2D line on image plane.  ${}^c\mathbf{L}_{[:3]}$  donates the first three rows of vector  ${}^c\mathbf{L}$ .

#### D. Key-Frame Selection

Observing that the learning-based data association method is able to track two frames which have large baseline, so different from frame-by-frame tracking strategy used in other VO or SLAM systems, we only match current frame with key-frames, as this can reduce the tracking error. A frame will be selected as a key-frame if any of the following conditions is satisfied:

- The distance to the last key-frame is larger than a given threshold  $\delta_d^{kf}$ .
- The angle with the last key-frame is larger than a given threshold  $\delta_\theta^{kf}$ .
- The number of tracked map-points is smaller than an upper threshold  $N_1^{kf}$  and bigger than a lower threshold  $N_2^{kf}$ .
- Tracked map-points are more than  $N_2^{kf}$  but the last frame tracking lost, i.e., map-points tracked by the last frame are less than  $N_2^{kf}$ .
- More than  $N_f^{kf}$  frames have passed since the last key-frame.

#### E. Graph Optimization

We select  $N_{kf}^{go}$  key-frames and construct a co-visibility graph similar to ORB-SLAM [17], where map-points, 3D lines, and key-frames are vertices and constraints are edges. Four kinds of constraints are utilized in the graph, including monocular line constraint, stereo line constraint, mono point constraint, and stereo point constraint.

1) *Monocular Line Constraint*: If only the left camera of frame  $k$  can observe the 3D line  ${}^w\mathbf{L}_i$ , then the re-projection error is defined as:

$$\mathbf{E}_{l_{k,i}}^m = e_l \left( {}^k\bar{\mathbf{l}}_i, {}^k\mathbf{P} ({}^c_w\mathbf{H} {}^w\mathbf{L}_i)_{[:3]} \right) \in \mathbb{R}^2, \quad (9a)$$

$$e_l \left( {}^k\bar{\mathbf{l}}_i, {}^k\mathbf{l}_i \right) = \left[ d \left( {}^k\mathbf{p}_{i,1}, {}^k\mathbf{l}_i \right) \quad d \left( {}^k\mathbf{p}_{i,2}, {}^k\mathbf{l}_i \right) \right]^T, \quad (9b)$$

where  ${}^k\bar{\mathbf{l}}_i$  is the observation of  ${}^w\mathbf{L}_i$  on frame  $k$ ,  $d(\mathbf{p}, \mathbf{l})$  is the distance between point  $\mathbf{p}$  and line  $\mathbf{l}$ , and  ${}^k\bar{\mathbf{p}}_{i,1}$  and  ${}^k\bar{\mathbf{p}}_{i,2}$  are the endpoints of  ${}^k\bar{\mathbf{l}}_i$ . Left camera is the main camera, so if only right camera observes a 3D line or point, the observation is not regarded as a constraint in our system.

2) *Stereo Line Constraint*: If both left camera and right camera of frame  $k$  can observe the 3D line  ${}^w\mathbf{L}_j$ , then the re-projection error is defined as:

$$\mathbf{E}_{l_{k,j}}^s = \begin{bmatrix} e_l \left( {}^k\bar{\mathbf{l}}_{j,l}, {}^k\mathbf{P} \begin{bmatrix} c \\ c_r \end{bmatrix} \mathbf{H} {}^w\mathbf{L}_j \right)_{[:3]} \\ e_l \left( {}^{k_r}\bar{\mathbf{l}}_{j,l}, {}^{k_r}\mathbf{P} \begin{bmatrix} c \\ c_r \end{bmatrix} \mathbf{H} {}^w\mathbf{L}_j \right)_{[:3]} \end{bmatrix} \in \mathbb{R}^4, \quad (10)$$

where  ${}^{k_r}\bar{\mathbf{l}}_j$  is the observation of  ${}^w\mathbf{L}_i$  on image captured by right camera of frame  $k$ .  ${}^{k_r}\mathbf{P}$  and  ${}^{c_r}\mathbf{H}$  are the line projection matrix and transformation matrix of right camera, respectively.

3) *Monocular Point Constraint*: If a 3D point  ${}^w\mathbf{X}_q$  is observed by only left camera of frame  $k$ , then the re-projection error is defined as:

$$\mathbf{E}_{p_{k,q}}^m = {}^k\bar{\mathbf{x}}_q^m - \pi_m \left( {}^c\mathbf{R} {}^w\mathbf{X}_q + {}^c\mathbf{t} \right), \quad (11)$$

where  ${}^k\bar{\mathbf{x}}_q^m = \left( {}^k\bar{u}_q, {}^k\bar{v}_q \right)$  is the observation of  ${}^w\mathbf{X}_q$  on frame  $k$  and  $\pi_m(\cdot)$  represents projecting a 3D point onto the image captured by left camera:

$$\pi_m \left( \begin{bmatrix} x \\ y \\ z \end{bmatrix} \right) = \begin{bmatrix} f_x \frac{x}{z} + c_x \\ f_y \frac{y}{z} + c_y \end{bmatrix}. \quad (12)$$

4) *Stereo Point Constraint*: If a 3D point  ${}^w\mathbf{X}_t$  is observed by both left camera and right camera of frame  $k$ , then the re-projection error is defined as:

$$\mathbf{E}_{p_{k,t}}^s = {}^k\bar{\mathbf{x}}_t^s - \pi_s \left( {}^c\mathbf{R} {}^w\mathbf{X}_t + {}^c\mathbf{t} \right), \quad (13)$$

where  ${}^k\bar{\mathbf{x}}_t^s = \left( {}^k\bar{u}_t, {}^k\bar{v}_t, {}^{k_r}\bar{u}_t \right)$  is the observation of  ${}^w\mathbf{X}_t$  on frame  $k$ ,  ${}^{k_r}\bar{u}_t$  is the horizontal coordinate in the right image, and  $\pi_s(\cdot)$  represents projecting a 3D point onto the stereo image:

$$\pi_s \left( \begin{bmatrix} x \\ y \\ z \end{bmatrix} \right) = \begin{bmatrix} f_x \frac{x}{z} + c_x \\ f_y \frac{y}{z} + c_y \\ f_x \frac{x-b}{z} + c_x \end{bmatrix}, \quad (14)$$

where  $b$  is the baseline between left camera and right camera.

5) *Cost Function*: Assuming that the observations obey Gaussian distribution, the final cost function can be defined as:

$$\begin{aligned} E = & \sum_{k,i} \rho_l^m \left( \left( \mathbf{E}_{l_{k,i}}^m \right)^T \Sigma_{l_{k,i}}^{-1} \left( \mathbf{E}_{l_{k,i}}^m \right) \right) \\ & + \sum_{k,j} \rho_l^s \left( \left( \mathbf{E}_{l_{k,j}}^s \right)^T \Sigma_{l_{k,j}}^{-1} \left( \mathbf{E}_{l_{k,j}}^s \right) \right) \\ & + \sum_{k,q} \rho_p^m \left( \left( \mathbf{E}_{p_{k,q}}^m \right)^T \Sigma_{p_{k,q}}^{-1} \left( \mathbf{E}_{p_{k,q}}^m \right) \right) \\ & + \sum_{k,t} \rho_p^s \left( \left( \mathbf{E}_{p_{k,t}}^s \right)^T \Sigma_{p_{k,t}}^{-1} \left( \mathbf{E}_{p_{k,t}}^s \right) \right), \end{aligned} \quad (15)$$

where  $\rho_l^m(\cdot)$ ,  $\rho_l^s(\cdot)$ ,  $\rho_p^m(\cdot)$ ,  $\rho_p^s(\cdot)$  are robust Huber cost functions and  $\Sigma_{l_{k,i}}^{-1}$ ,  $\Sigma_{l_{k,j}}^{-1}$ ,  $\Sigma_{p_{k,q}}^{-1}$ ,  $\Sigma_{p_{k,t}}^{-1}$  are the inverse covariance matrices, respectively.

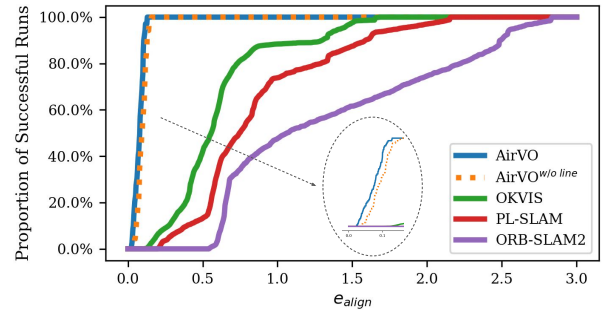


Fig. 5: A comparison on on OIVIO MN\_050\_GV\_02 sequence. The vertical axis is the proportion of successful runs, as determined by the given alignment error threshold on the horizontal axis.

## IV. EXPERIMENTS

In this section, experimental results will be presented to demonstrate the performance of our method. We takes pre-trained SuperPoint and SuperGlue to detect and match feature points without any fine-tuning. The experiments are conducted on two datasets: OIVIO dataset [51] and UMA visual-inertial dataset [6]. We compare the localization accuracy of the proposed method with PL-SLAM [26], VINS-Fusion [3], StructVIO [34], UV-SLAM [30], and Stereo ORB-SLAM2 [19]. As the proposed method is a VO system, we disabled the loop closure part from above baselines. Note that we cannot compare with DX-SLAM [15] and GCNv2-SLAM [22], since they are based on RGB-D inputs.

### A. Results on OIVIO Benchmark

OIVIO dataset collects visual-inertial data in tunnels and mines. In each sequence, the scene is illuminated by an onboard light of approximately 1300, 4500, or 9000 lumens. We selected all the nine sequences with ground-truth acquired by the Leica TCRP1203 R300. The performance of translational error is presented in Table I. The two most accurate results are **highlighted** and underlined, respectively. AirVO achieves the best performance on 6 sequences and the second best performance on other 3 sequences, which outperforms other state-of-the-art algorithms. We notice that VINS-Fusion, StructVIO and UV-SLAM track lost on many sequences, this may be because their feature tracking methods, i.e., KLT sparse optical flow, ZNCC, LBD descriptor, are not illumination-robust. To show the effectiveness of the proposed line processing method, we remove line features from AirVO and name it as AirVO<sup>w/o line</sup>. It can be seen that the average translational error decreases 13.2% after adding line features, which verifies that employing lines can improve the accuracy of our system.

We show a comparison of our method with selected baselines on OIVIO MN\_050\_GV\_02 sequence in Fig. 5. In this case, the robot goes through a mine with onboard illumination. The travelling distance is about 83 meters and the average speed is about 0.5m/s. The plot shows the proportion of successful runs on the vertical axis, as determined by the

TABLE I: Translational error (RMSE) without loop closing on the OIVIO dataset (unit: m). **L** refers to tracking lost and **D** refers to sequences where RMSEs are larger than 10m.

Sequence	VINS-Fusion	Struct-VIO	UV-SLAM	PL-SLAM	OKVIS	ORB-SLAM2	AirVO <sup>w/o line</sup>	AirVO
MN_015_GV_01	0.1033	8.6098	0.4991	1.3166	0.0663	3.6847	0.0618	<b>0.0584</b>
MN_015_GV_02	<b>D</b>	<b>L</b>	<b>D</b>	0.9523	1.5320	1.5767	<u>0.0830</u>	<b>0.0682</b>
MN_050_GV_01	<b>D</b>	<b>D</b>	<b>D</b>	1.1538	0.7785	3.4891	<u>0.0895</u>	<b>0.0624</b>
MN_050_GV_02	<b>D</b>	<b>D</b>	<b>D</b>	1.0055	0.7385	1.6392	<u>0.0940</u>	<b>0.0765</b>
MN_100_GV_01	<b>D</b>	<b>D</b>	<b>D</b>	0.8455	0.8729	3.6059	<b>0.0566</b>	<u>0.0570</u>
MN_100_GV_02	<b>D</b>	<b>D</b>	<b>D</b>	0.6708	0.4360	1.5259	<b>0.0604</b>	<u>0.0681</u>
TN_015_GV_01	<b>0.1541</b>	7.5849	1.6695	1.8856	0.3063	2.1966	0.1861	<u>0.1714</u>
TN_050_GV_01	0.2079	<b>D</b>	2.5948	1.9335	0.2262	2.0384	<u>0.1472</u>	<b>0.1035</b>
TN_100_GV_01	0.4063	<b>D</b>	1.4496	1.5263	0.3984	2.3370	<u>0.1088</u>	<b>0.0988</b>



Fig. 6: A small challenging sequence in UMA-VI dataset. The image may suddenly darken as a result of turning off the lights.

TABLE II: Translational error (RMSE) without loop closing on the UMA-VI dataset (unit: m). The best results are **highlighted**.

Sequence	PL-SLAM	OKVIS	AirVO <sup>w/o line</sup>	AirVO
conference-csc1	2.6974	1.1181	1.9806	<b>1.0781</b>
conference-csc2	1.5956	0.4696	0.1440	<b>0.1370</b>
third-floor-csc1	4.4779	0.2525	0.1273	<b>0.1044</b>
third-floor-csc2	6.0675	0.2161	0.1315	<b>0.1265</b>
average	3.7096	0.5141	0.5959	<b>0.3615</b>

alignment error threshold on the horizontal axis. AirVO achieves the most accurate result on this sequence.

### B. Results on UMA-VI Benchmark

UMA-VI dataset is a visual-inertial dataset gathered in illumination-challenging scenarios with handheld custom sensors. We use sequences with illumination changes to evaluate our system. As shown in Fig. 6, it contains many sub-sequences where the image suddenly darkens as a result of turning off the lights. It's more challenging than OIVIO dataset, so we only select methods proved to be illumination-robust in Section IV-A as baselines, i.e., PL-SLAM, OKVIS and AirVO<sup>w/o line</sup>. The translational errors are presented in Table II. It can be seen that AirVO outperforms other methods. Its average translational error is only 9.8% of PL-SLAM, 61.0% of AirVO<sup>w/o line</sup> and 70.7% of OKVIS. We notice that the aligned errors are larger than those on OIVIO dataset. It's because UMA-VI dataset only gives ground-truth of the beginning and ending of each sequence, and the scenes are more difficult for VO or VIO systems.

We also compare the trajectory of AirVO with OKVIS

and PL-SLAM on conference-csc2 sequence as shown in Fig. 1. The traveling distance of this sequence is about 50 meters and average speed is about 0.75m/s. It clearly shows that AirVO produces the best accuracy in this challenging case. The drift error of AirVO is about 0.58%. OKVIS and PL-SLAM are 1.6% and 8.1%, respectively.

### C. Runtime Analysis

This section presents the runtime of the proposed system. The evaluation is performed on a laptop with an AMD Ryzen Threadripper PRO 3975WX processor and a NVIDIA Geforce RTX 3090 GPU. The resolution of input image is 752 × 480. We first verify the acceleration of point detection and matching network. In our system, detecting and tracking feature points for one image take 15ms, and the original python code needs 40ms. So time cost is further reduced by 62.5%. Then we present the running time of each module in Table III. Notice that the feature detection module includes detecting points and lines for stereo images. The tracking module includes stereo matching and frame-to-frame feature tracking. It can be seen that the whole system can run in real time (20 FPS).

TABLE III: Runtime Analysis.

Module	Feature Detection	Tracking	Pose Estimation	Overall
Time	20.8 ms	20.0 ms	3.9 ms	48 ms

## V. CONCLUSIONS

In this work, we presented an illumination-robust visual odometry based on learning based key-point detection and matching methods. To improve the accuracy, line features are also utilized in our system. We proposed a novel line matching method to make line tracking robust enough in dynamic environments. In the experiments, we showed that the proposed method achieved superior performance in dynamic illumination environments and could run in real time. We open the source code and expect this method will play an important role in robotic applications. For future work, we will extend AirVO to a SLAM system by adding loop closing, re-localization and map-reuse. We hope to build an illumination-robust visual map for long-term localization.

## REFERENCES

- [1] A. Macario Barros, M. Michel, Y. Moline, G. Corre, and F. Carrel, "A comprehensive survey of visual slam algorithms," *Robotics*, vol. 11, no. 1, p. 24, 2022.
- [2] A. I. Mourikis, S. I. Roumeliotis *et al.*, "A multi-state constraint kalman filter for vision-aided inertial navigation." in *ICRA*, vol. 2, 2007, p. 6.
- [3] T. Qin, P. Li, and S. Shen, "Vins-mono: A robust and versatile monocular visual-inertial state estimator," *IEEE Transactions on Robotics*, vol. 34, no. 4, pp. 1004–1020, 2018.
- [4] S. Leutenegger, P. Furgale, V. Rabaud, M. Chli, K. Konolige, and R. Siegwart, "Keyframe-based visual-inertial slam using nonlinear optimization," *Proceedings of Robotis Science and Systems (RSS) 2013*, 2013.
- [5] C. Cadena, L. Carlone, H. Carrillo, Y. Latif, D. Scaramuzza, J. Neira, I. Reid, and J. J. Leonard, "Past, present, and future of simultaneous localization and mapping: Toward the robust-perception age," *IEEE Transactions on robotics*, vol. 32, no. 6, pp. 1309–1332, 2016.
- [6] D. Zuñiga-Noël, A. Jaenal, R. Gomez-Ojeda, and J. Gonzalez-Jimenez, "The uma-vi dataset: Visual-inertial odometry in low-textured and dynamic illumination environments," *The International Journal of Robotics Research*, vol. 39, no. 9, pp. 1052–1060, 2020.
- [7] K. Xu, C. Wang, C. Chen, W. Wu, and S. Scherer, "Aircode: A robust object encoding method," *IEEE Robotics and Automation Letters*, vol. 7, no. 2, pp. 1816–1823, 2022.
- [8] K. M. Yi, E. Trulls, V. Lepetit, and P. Fua, "Lift: Learned invariant feature transform," in *European conference on computer vision*. Springer, 2016, pp. 467–483.
- [9] D. DeTone, T. Malisiewicz, and A. Rabinovich, "Superpoint: Self-supervised interest point detection and description," in *Proceedings of the IEEE conference on computer vision and pattern recognition workshops*, 2018, pp. 224–236.
- [10] C. B. Choy, J. Gwak, S. Savarese, and M. Chandraker, "Universal correspondence network," *Advances in neural information processing systems*, vol. 29, 2016.
- [11] P.-E. Sarlin, D. DeTone, T. Malisiewicz, and A. Rabinovich, "Superglue: Learning feature matching with graph neural networks," in *Proceedings of the IEEE/CVF conference on computer vision and pattern recognition*, 2020, pp. 4938–4947.
- [12] D. G. Viswanathan, "Features from accelerated segment test (fast)," in *Proceedings of the 10th workshop on image analysis for multimedia interactive services, London, UK, 2009*, pp. 6–8.
- [13] E. Rublee, V. Rabaud, K. Konolige, and G. Bradski, "Orb: An efficient alternative to sift or surf," in *2011 International conference on computer vision*. Ieee, 2011, pp. 2564–2571.
- [14] P.-E. Sarlin, C. Cadena, R. Siegwart, and M. Dymczyk, "From coarse to fine: Robust hierarchical localization at large scale," in *Proceedings of the IEEE/CVF Conference on Computer Vision and Pattern Recognition*, 2019, pp. 12716–12725.
- [15] D. Li, X. Shi, Q. Long, S. Liu, W. Yang, F. Wang, Q. Wei, and F. Qiao, "Dxslam: A robust and efficient visual slam system with deep features," in *2020 IEEE/RSJ International Conference on Intelligent Robots and Systems (IROS)*. IEEE, 2020, pp. 4958–4965.
- [16] S. Leutenegger, M. Chli, and R. Y. Siegwart, "Brisk: Binary robust invariant scalable keypoints," in *2011 International conference on computer vision*. Ieee, 2011, pp. 2548–2555.
- [17] R. Mur-Artal, J. M. M. Montiel, and J. D. Tardos, "Orb-slam: a versatile and accurate monocular slam system," *IEEE transactions on robotics*, vol. 31, no. 5, pp. 1147–1163, 2015.
- [18] T. Schneider, M. Dymczyk, M. Fehr, K. Egger, S. Lynen, I. Gilitschenski, and R. Siegwart, "maplab: An open framework for research in visual-inertial mapping and localization," *IEEE Robotics and Automation Letters*, vol. 3, no. 3, pp. 1418–1425, 2018.
- [19] R. Mur-Artal and J. D. Tardós, "Orb-slam2: An open-source slam system for monocular, stereo, and rgb-d cameras," *IEEE transactions on robotics*, vol. 33, no. 5, pp. 1255–1262, 2017.
- [20] R. Kang, J. Shi, X. Li, Y. Liu, and X. Liu, "Df-slam: A deep-learning enhanced visual slam system based on deep local features," *arXiv preprint arXiv:1901.07223*, 2019.
- [21] V. Balntas, E. Riba, D. Ponsa, and K. Mikolajczyk, "Learning local feature descriptors with triplets and shallow convolutional neural networks," in *Bmvc*, vol. 1, no. 2, 2016, p. 3.
- [22] J. Tang, L. Ericson, J. Folkesson, and P. Jensfelt, "Gcnv2: Efficient correspondence prediction for real-time slam," *IEEE Robotics and Automation Letters*, vol. 4, no. 4, pp. 3505–3512, 2019.
- [23] X. Han, Y. Tao, Z. Li, R. Cen, and F. Xue, "Superpointvo: A lightweight visual odometry based on cnn feature extraction," in *2020 5th International Conference on Automation, Control and Robotics Engineering (CACRE)*. IEEE, 2020, pp. 685–691.
- [24] H. M. S. Bruno and E. L. Colombini, "Lift-slam: A deep-learning feature-based monocular visual slam method," *Neurocomputing*, vol. 455, pp. 97–110, 2021.
- [25] J. L. Schonberger and J.-M. Frahm, "Structure-from-motion revisited," in *Proceedings of the IEEE conference on computer vision and pattern recognition*, 2016, pp. 4104–4113.
- [26] R. Gomez-Ojeda, F.-A. Moreno, D. Zuniga-Noël, D. Scaramuzza, and J. Gonzalez-Jimenez, "Pl-slam: A stereo slam system through the combination of points and line segments," *IEEE Transactions on Robotics*, vol. 35, no. 3, pp. 734–746, 2019.
- [27] X. Zuo, X. Xie, Y. Liu, and G. Huang, "Robust visual slam with point and line features," in *2017 IEEE/RSJ International Conference on Intelligent Robots and Systems (IROS)*. IEEE, 2017, pp. 1775–1782.
- [28] Y. Yang, P. Geneva, K. Eickenhoff, and G. Huang, "Visual-inertial odometry with point and line features," in *2019 IEEE/RSJ International Conference on Intelligent Robots and Systems (IROS)*. IEEE, 2019, pp. 2447–2454.
- [29] X. Li, Y. He, J. Lin, and X. Liu, "Leveraging planar regularities for point line visual-inertial odometry," in *2020 IEEE/RSJ International Conference on Intelligent Robots and Systems (IROS)*. IEEE, 2020, pp. 5120–5127.
- [30] H. Lim, J. Jeon, and H. Myung, "Uv-slam: Unconstrained line-based slam using vanishing points for structural mapping," *IEEE Robotics and Automation Letters*, vol. 7, no. 2, pp. 1518–1525, 2022.
- [31] L. Zhang and R. Koch, "An efficient and robust line segment matching approach based on lbd descriptor and pairwise geometric consistency," *Journal of Visual Communication and Image Representation*, vol. 24, no. 7, pp. 794–805, 2013.
- [32] R. G. Von Gioi, J. Jakubowicz, J.-M. Morel, and G. Randall, "Lsd: A line segment detector," *Image Processing On Line*, vol. 2, pp. 35–55, 2012.
- [33] L. Zhou, S. Wang, and M. Kaess, "Dplvo: Direct point-line monocular visual odometry," *IEEE Robotics and Automation Letters*, vol. 6, no. 4, pp. 7113–7120, 2021.
- [34] D. Zou, Y. Wu, L. Pei, H. Ling, and W. Yu, "Structvio: visual-inertial odometry with structural regularity of man-made environments," *IEEE Transactions on Robotics*, vol. 35, no. 4, pp. 999–1013, 2019.
- [35] B. Xu, P. Wang, Y. He, Y. Chen, Y. Chen, and M. Zhou, "Leveraging structural information to improve point line visual-inertial odometry," *IEEE Robotics and Automation Letters*, vol. 7, no. 2, pp. 3483–3490, 2022.
- [36] L. Di Stefano, S. Mattoccia, and F. Tombari, "Zncc-based template matching using bounded partial correlation," *Pattern recognition letters*, vol. 26, no. 14, pp. 2129–2134, 2005.
- [37] S. Klose, P. Heise, and A. Knoll, "Efficient compositional approaches for real-time robust direct visual odometry from rgb-d data," in *2013 IEEE/RSJ International Conference on Intelligent Robots and Systems*. IEEE, 2013, pp. 1100–1106.
- [38] J. Engel, J. Stückler, and D. Cremers, "Large-scale direct slam with stereo cameras," in *2015 IEEE/RSJ international conference on intelligent robots and systems (IROS)*. IEEE, 2015, pp. 1935–1942.
- [39] J. Engel, V. Koltun, and D. Cremers, "Direct sparse odometry," *IEEE transactions on pattern analysis and machine intelligence*, vol. 40, no. 3, pp. 611–625, 2017.
- [40] G. G. Scandaroli, M. Meilland, and R. Richa, "Improving ncc-based direct visual tracking," in *European conference on Computer Vision*. Springer, 2012, pp. 442–455.
- [41] A. Crivellaro and V. Lepetit, "Robust 3d tracking with descriptor fields," in *Proceedings of the IEEE Conference on Computer Vision and Pattern Recognition*, 2014, pp. 3414–3421.
- [42] H. Alismail, B. Browning, and S. Lucey, "Direct visual odometry using bit-planes," *arXiv preprint arXiv:1604.00990*, 2016.
- [43] Q. Gu, P. Liu, J. Zhou, X. Peng, and Y. Zhang, "Drms: Dim-light robust monocular simultaneous localization and mapping," in *2021 International Conference on Computer, Control and Robotics (ICCCR)*. IEEE, 2021, pp. 267–271.
- [44] L. Yu, E. Yang, and B. Yang, "Afe-orb-slam: robust monocular vslam based on adaptive fast threshold and image enhancement for complex lighting environments," *Journal of Intelligent & Robotic Systems*, vol. 105, no. 2, pp. 1–14, 2022.

- [45] A. Savinykh, M. Kurenkov, E. Kruzhkov, E. Yudin, A. Potapov, P. Karpyshev, and D. Tsetserukou, "Darkslam: Gan-assisted visual slam for reliable operation in low-light conditions," *arXiv preprint arXiv:2206.02199*, 2022.
- [46] S. Park, T. Schöps, and M. Pollefeys, "Illumination change robustness in direct visual slam," in *2017 IEEE international conference on robotics and automation (ICRA)*. IEEE, 2017, pp. 4523–4530.
- [47] J. Huang and S. Liu, "Robust simultaneous localization and mapping in low-light environment," *Computer Animation and Virtual Worlds*, vol. 30, no. 3-4, p. e1895, 2019.
- [48] P. Kim, H. Lee, and H. J. Kim, "Autonomous flight with robust visual odometry under dynamic lighting conditions," *Autonomous Robots*, vol. 43, no. 6, pp. 1605–1622, 2019.
- [49] Z. Chen and C. Heckman, "Robust pose estimation based on normalized information distance," in *2021 IEEE/RSJ International Conference on Intelligent Robots and Systems (IROS)*. IEEE, 2021, pp. 2217–2223.
- [50] A. Bartoli and P. Sturm, "Structure-from-motion using lines: Representation, triangulation, and bundle adjustment," *Computer vision and image understanding*, vol. 100, no. 3, pp. 416–441, 2005.
- [51] M. Kasper, S. McGuire, and C. Heckman, "A benchmark for visual-inertial odometry systems employing onboard illumination," in *2019 IEEE/RSJ International Conference on Intelligent Robots and Systems (IROS)*. IEEE, 2019, pp. 5256–5263.